11th World Congress on Computational Mechanics (WCCM XI)
5th European Conference on Computational Mechanics (ECCM V)
6th European Conference on Computational Fluid Dynamics (ECFD VI)
E. Oñate, J. Oliver and A. Huerta (Eds)

NUMERICAL MODELLING OF GEOMETRICAL EFFECTS IN THE PERFORMANCE OF A CYCLOIDAL ROTOR

C. M. Xisto[1,*], J. C. Páscoa[1], J. A. Leger[1], P. Masarati[2], G. Quaranta[2], M. Morandini[2], L. Gagnon[2], D. Wills[3] and M. Schwaiger[3]

[1] Dep. de Eng. Electromecânica, Universidade da Beira Interior - Centre for Aerospace Science and Technology. Rua Mq.s D'Ávila e Bolama, 6201-001 Covilhã, Portugal
xisto@ubi.pt; pascoa@ubi.pt; http://clusterdem.ubi.pt; www.crop-project.eu
[2] Dipartimento di Scienze e Tecnologie Aerospaziali, Politecnico di Milano, via La Masa 34, 20156 Milano, Italy
[3]IAT21-Innovative Aeronautics Technologies GmbH, Langholzstraße 16, A-4050 Traun, Austria

Key words: CROP, Aerodynamics, Parametric, CFD, Cyclorotor.

Abstract. *In the following paper we perform an unsteady CFD analysis of the effect of several two dimensional blade geometrical parameters in the performance of CROP. The values will be analysed in terms of power loading (Thrust/Power) vs Disk Load (Thrust/Disk Area). The geometric parameters that we investigate include: blade thickness; rotor solidity (number of blades); and pitching amplitude.*

1 INTRODUCTION

The CROP (Cycloidal Rotor Optimized for Propulsion) project strives to design a radically different new and "Green" propulsion system for manned and unmanned aerial vehicles. The CROP concept is based on a rotating wing system, where the axis of rotation is parallel to the blade span, see Fig. 1-a). The blades pitching schedule is controlled by a mechanical system that is able to change the direction and magnitude of the rotor resultant thrust vector, thus allowing for a substantial increase in the aircraft maneuverability (Fig. 1-b)). CROP introduces several potential advantages in comparison with traditional VTOL or fixed wing air vehicles. It uses common surfaces to achieve lift and thrust along the full range of flight speeds. The use of a wing rotating around the axial axis creates lift, and thrust, when the blades move backward in relation to the vehicle's direction of flight. This makes possible to use the intermittent, but very high, lift value generated by the unsteady pitching of the blades. Further, each blade of the cyclorotor (CR) operates at similar conditions (angle of attack, velocity, Reynolds number) so, in principle, the blades are easier to optimize in terms of aerodynamic performance [4]. The unsteady flow mechanism that is generated by the pitching movement of the blades also plays a significant role in the aerodynamic efficiency of the CR, since it can delay blade

stall, thus increasing the amount of lift that can be produced by each blade. Moreover, the rotational speed and pitching schedule of the CR does not need to increase with vehicle speed, since the achievable thrust increases with forward airspeed for a constant rotor angular velocity. The analysis of this kind of complex flows can be performed using numerical gas dynamic codes [8, 11, 12].

In the following paper we perform an unsteady CFD analysis of the effect of several 2D blade geometrical parameters in the performance of CROP. The results will be analysed in terms of power loading (Thrust/Power) vs Disk Load (Thrust/Disk Area). The geometric parameters that we investigate include: blade thickness; rotor solidity (number of blades); and pitching amplitude. This analysis was already done by several authors [13, 5, 3, 2] for MAV scale cyclorotors, while here we intend to extend such study for large scale systems that could be implemented in manned aircrafts. In a previous paper an analytical parametric study of the rotor behavior in motion was performed by Leger et al. [6, 7], here we want to analyze the geometrical effects when the rotor is in a hovering state.

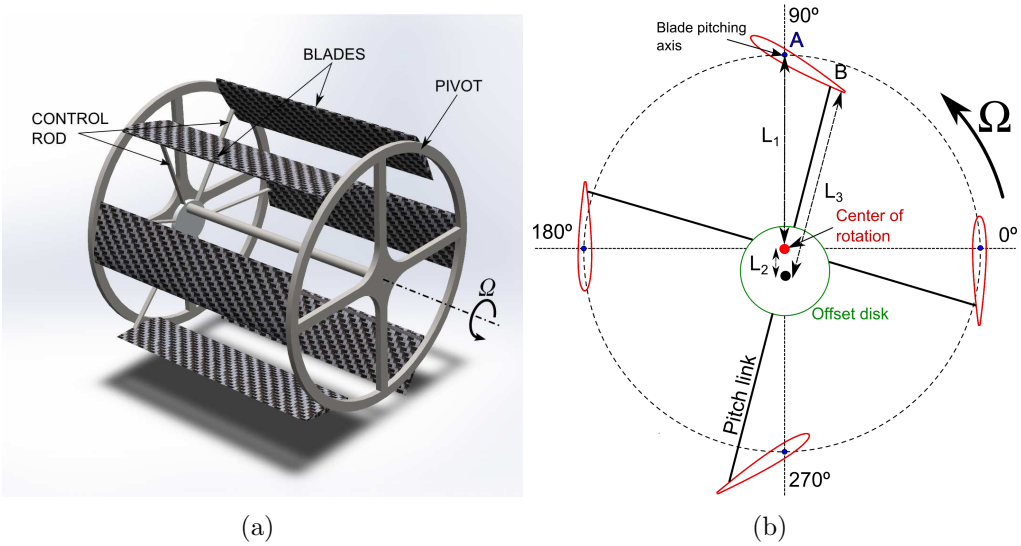

(a) (b)

Figure 1: a) 3D representation of a cyclorotor with six NACA0012 blades and a maximum pitch angle of 40 degree b) Possible configuration for the pitch control mechanism, adapted form [4].

2 VALIDATION

For validation we have computed the IAT21 L3 Cycloidal Rotor (CR) configuration and compared the numerical solution with the available experimental data [9]. The L3 CR comprises six NACA0016 blades with a chord/radius ratio equal to 0.5, see Fig. 2-a). The pitching axis is located at 35% of chord and the blade span is equal to the rotor diameter, the distance between the pitching axis is $d = 0.120$ m. The pitching schedule results in an asymmetric pitching profile that varies from +36 deg, in the top section of

the rotor ($\Psi = 90$ deg), to -39 deg, in the bottom section of the rotor ($\Psi = 270$ deg). This blade pitch angle variation is given by a four bar linkage mechanism,

$$\theta = \frac{\pi}{2}\sin^{-1}\left[\frac{e}{a}\cos\left(\Psi+\varepsilon\right)\right] - \cos^{-1}\left(\frac{a^2+d^2-L^2}{2ad}\right), \tag{1}$$

where,

$$a^2 = e^2 + R^2 - 2eR\cos\left(\Psi+\epsilon+\frac{\pi}{2}\right). \tag{2}$$

The angular velocity, ω, of the pitching blades is given by:

$$\omega = \frac{d\theta}{d\Psi}\Omega. \tag{3}$$

The computed pitching movement of the blades was calculated with (3). The values for the control rod length ($L = 0.61$ m), for the magnitude of eccentricity ($e = 0.073$ m) and for the phase angle ($\varepsilon = 0$ deg) are estimated in order to obtain the desired pitching profile. In Fig. 2-b) we show the numerical grid used for the computation of the IAT21 L3 rotor. The numerical domain has a circular shape with radius equal to 20 m and a total of 306653 cells. In Fig. 2-c) we show the rotor grid at $t = 0$ s, and in Fig. 2-d) a detail view of one of the blades grid ($\Psi = 60$ deg) is presented. For the blades we have generated a hybrid mesh with a structured O-type grid in the boundary layer region ($y^+ < 1$) and an unstructured grid in the remaining computational domain. The blade numerical domain exchanges information with the rotor domain through a simple grid interface. The rotor is rotating with constant angular velocity (Ω) and also communicates with the environment domain ($\Omega = 0$ rad/s) through a grid interface. The unsteady solution was computed for a rotor rotation of 0.5 deg per time step.

For solving the incompressible Navier-Stokes equations we have used a pressure-coupled-based solver, with a second order implicit time discretization. For variable interpolation we applied the second order linear upwind differencing scheme. Turbulent effects were modeled by the one-equation Spalart-Allmaras model. Regarding boundary conditions we impose a non-slip boundary condition in the walls and we extrapolate the variables at the outlet. The rotation of the rotor and the pitching movement of the blades results from the sliding mesh technique.

In Fig. 3 we show a comparison between the computed results and experimental data for the L3 rotor configuration. We can see that the current model overestimate thrust and underestimate power consumption, although the trend of computational and experimental results is the same. The over estimation of thrust could be related to the fact that this is a 2D approximation of the rotor and the 3D losses are being neglected. The under estimation of power should be related to the fact that we only compute the aerodynamic component of the overall power (this means that we do not account for the parasite power, required to rotate the rotor frame) and again the 3D losses are not being taken into account.

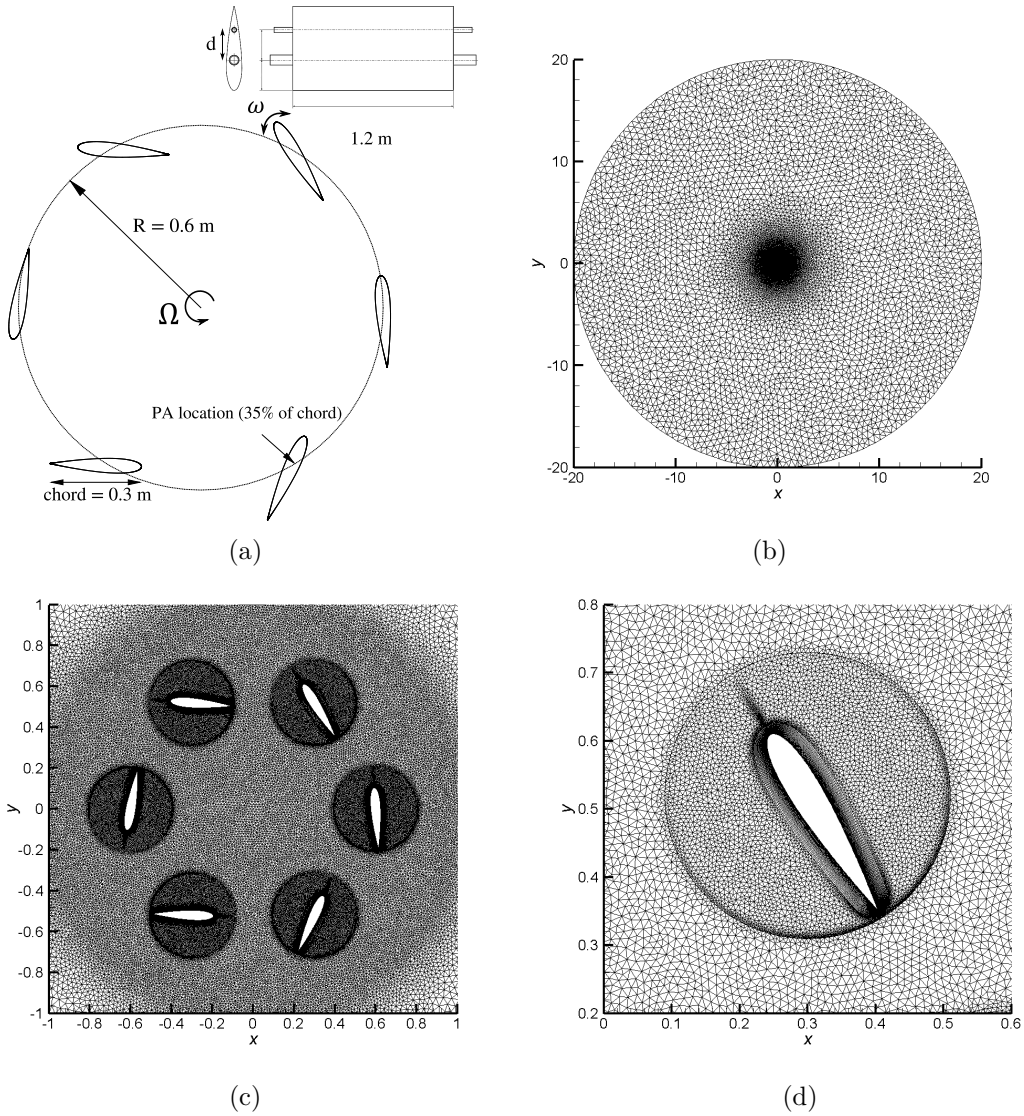

Figure 2: a)IAT21 L3 rotor configuration. Numerical grid used for the computation of the IAT21 L3 rotor: b) Global view of the mesh; c) Detail view of the rotor; d) Detail view of one blade.

3 PARAMETRIC STUDY

In the following section we present a parametric CFD analysis of several rotor geometrical parameters. We start with a blade profile analysis, in which we address the effect of airfoil thickness in the performance of CROP. Afterwards we analyse the influence of increasing the rotor solidity, that is given by adding more blades (constant chord) into the rotor.

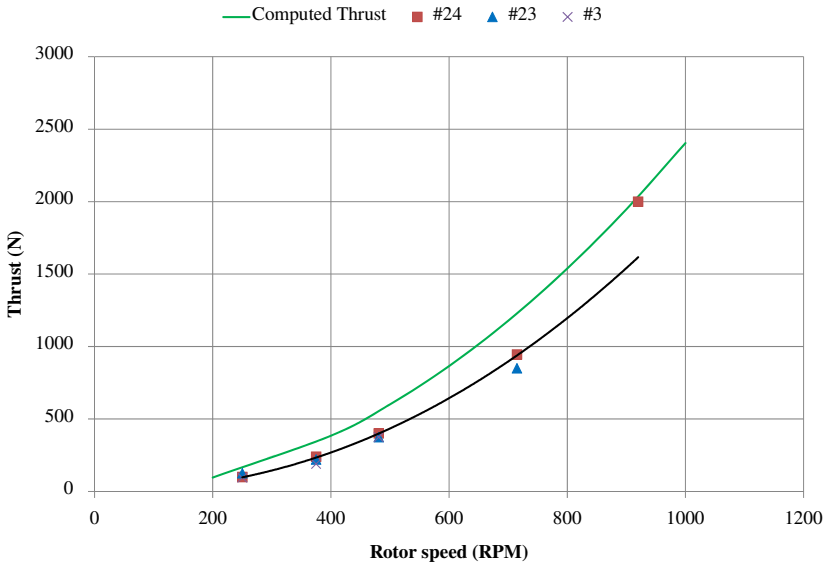

(a)

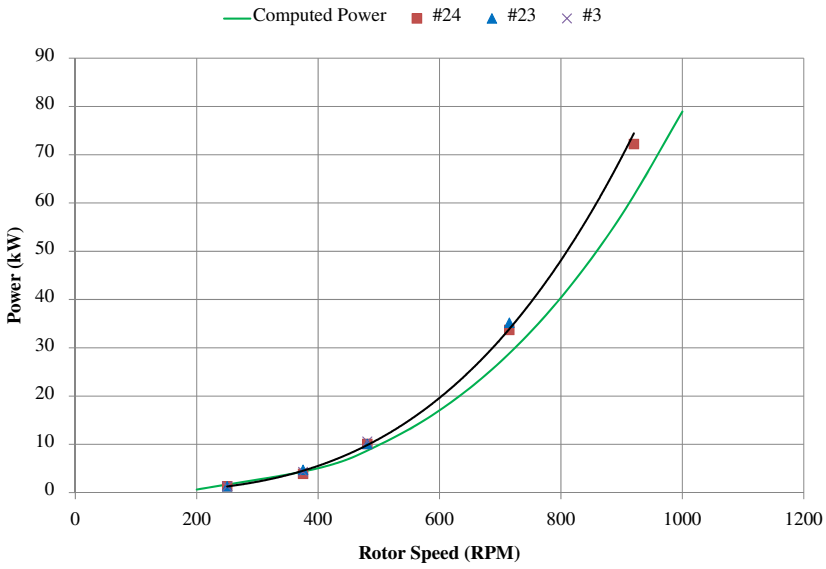

(b)

Figure 3: a) Comparison between the computed Thrust (a) and power (b) with experimental data for the L3 rotor configuration.

3.1 Blade profile analysis

As we increase the rotor dimensions, the airfoil section could have a significant role in the aerodynamic performance. In this section we analyze the effect of airfoil thickness

Table 1: Rotor dimensions for the blade profile analysis.

Airfoil	**NACA0006;0010;0015;0018**
Rotor Diameter (m)	1
Span, S (m)	1
Chord,c (m)	0.25
Pitching axis location (m)	25% of chord
Number of Blade	4
Maximum Pitch Angle (deg)	40
Minimum Pitch Angle (deg)	-40
Rotation Speed (RPM)	200, 400, 600, 800

for several rotation speeds. This study was already performed for MAV scale cyclorotors, here we intend to extend this analysis for large scale rotors which are capable of producing enough thrust for small size manned aircrafts. The rotor dimensions are shown in Table 1. The rotor diameter and span are equal to 1 m and the blade chord is equal to 0.25 m. We have analyzed four different configurations with airfoil increasing thickness, namely the NACA0006;0010;0015;0018. The pitch angle amplitude lies between 40 deg and -40 deg, and an ideal pitch angle equation was used to described the oscillatory movement of the blades,

$$\theta = \alpha_0 \cdot \sin(\Omega t + \Psi_0), \tag{4}$$

the time derivative gives us the angular pitching velocity of the blades,

$$\omega = \dot{\theta} = \alpha_0 \cdot \Omega \cdot \cos(\Omega t + \Psi_0), \tag{5}$$

where $\alpha_0 = 40$ deg is the pitch amplitude and Ψ_0 is the initial blade position. The rotor rotates in the counterclockwise direction and the pitching axis is located at 25% of the chord.

The numerical domain is 2D with a circular shape ($R = 20$m). In order to proper solve the boundary layer, in these regions the mesh is again hybrid with a structured O-type grid in the boundary layer region and an unstructured grid in the remaining numerical domain. Each one of the computed CRs is composed by four sub-blocks (blades) that should obey to Eqn. (5). These sub-blocks communicate with the rotating rotor with a grid interface and the rotor will also exchange information with the stationary environment. For computing the flow we have used the same solvers and models of the previous section.

In Fig. 4 we show the Power Loading (Thrust/Power) vs Disk load (Thrust/disk Area). We can see that, as we increase the thickness of the airfoil, the power loading also increases for all values of disk load. This is because not only the thrust increases but also the power requirement decreases with an increase of thickness. In order to understand the mechanism that is behind this improvement in the rotor efficiency, we have plotted the streamlines for the relative velocity in Fig. 3. We can observe that for the NACA0006 rotor, the flow is separated when each one of the four blades is in the top rotor position. As

we increase the thickness the recirculation zone size is reduced, and it is almost negligible in the NACA0018 test case. This is a direct consequence of the virtual camber effect.

Camber effect can introduce significant changes in the behaviour of the angle of attack of each blade. Rotating velocity will affect each point along the blade chord line, since each one of these points will have a different local velocity as a consequence of the superimposition of the (steady) rotor angular velocity and of the (harmonic) blade pitch velocity. This effect will result in a top position negative equivalent camber and bottom position positive equivalent camber. Its consequence is a larger force generated by the bottom blade when compared with top blade of the rotor (negative lift can also be obtained here). It plays a significant role in the aerodynamic behaviour of the cyclorotor. One solution could be the incorporation of cambered blades in the rotor. However we know that in a cyclorotor the blades need to operate at positive and negative angles of attack. This means that if we have a positive camber in the upper surface of the rotor we will have a negative camber in the lower surface. This effect will be responsible for a drop on rotor performance and can generate stall conditions for the lower blade position. Nevertheless, cambered blades can improve rotor performance if the camber can be changed in the upper and lower half of the rotating cycle. Flow separation can also be reduced, or avoid, with the inclusion of active flow control techniques such Dielectric Barrier Discharge (DBDs) plasma actuators [1, 10].

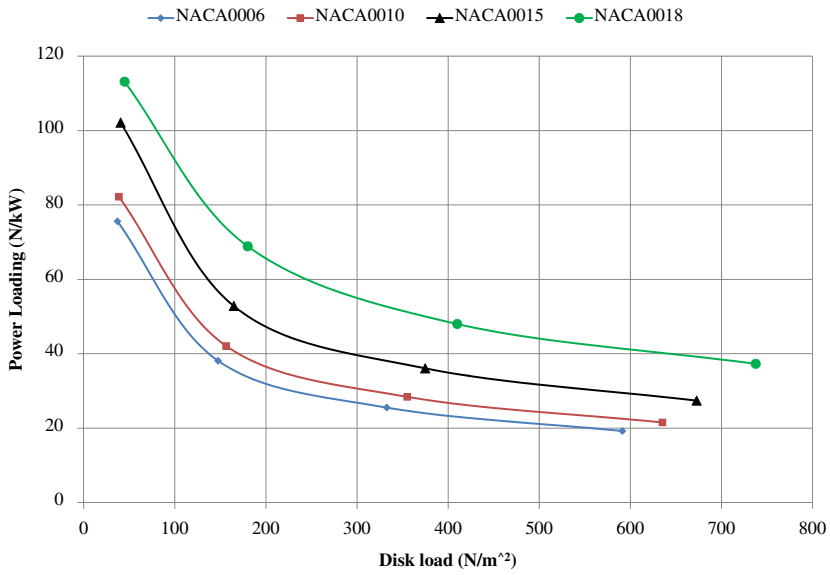

Figure 4: Power Loading vs Disk Load results for the blade profile analysis.

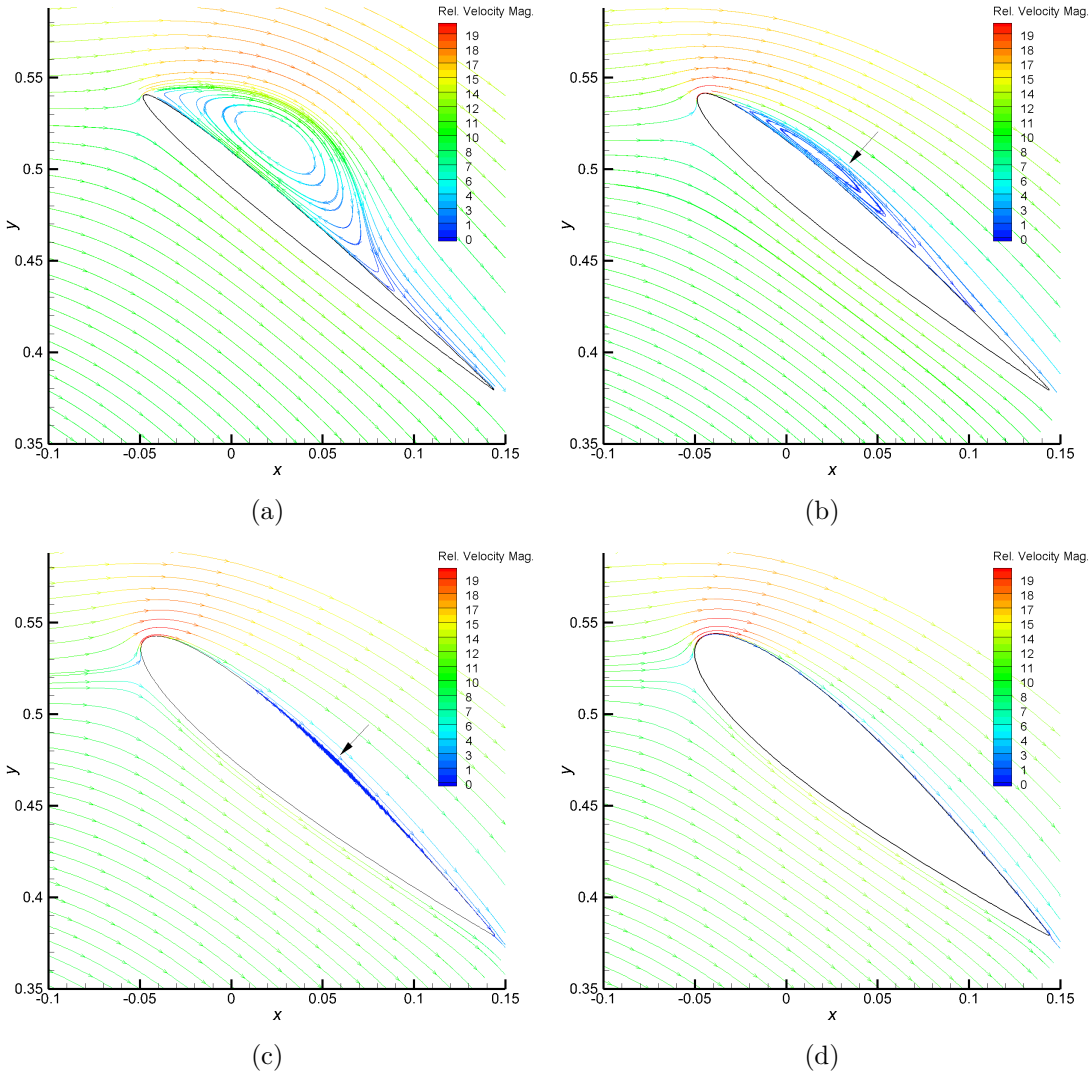

Figure 5: Streamlines for the relative velocity @200RPM a) NACA0006; b) NACA0010; c) NACA0015; d) NACA0018.

3.2 Rotor Solidity

The second test case is related to the rotor solidity at constant blade chord and span. This means increasing the rotor solidity just by increasing the number of blades. This study should allow us to find an optimum value for the number of rotor blades for a specific thrust and pitch amplitude, until the interference effects come into play. For a cycloidal rotor, solidity is defined as

$$\sigma = \frac{N \cdot c}{2\pi r}, \tag{6}$$

Notice that we can increase solidity just by increasing the chord, c, or the number of blades (N). For this analysis we have chosen the NACA0018 blade since it was the airfoil that performed better in the previous section. We have used the same rotor parameters of Table 1 with the exception that now the blade profile is fixed and the number of rotor blades varies.

In Fig. 6 we show the plot for the power loading results as a function of disk load. We can see that the 3-bladed rotor is showing higher values of power loading, so in principle this should be the optimal rotor for pitch amplitude of 40 deg. However, since we can achieve higher thrust with the 4 blade configuration, for applications where power consumption is not a factor, we should go for the four bladed rotor. When two more blades are added to the rotor (6 blades) the interference effects come into play and the rotor power loading, and even the trust capability, is highly deteriorated

Figure 8 shows the velocity magnitude contours for each one of the analysed 40 deg pitch configurations. In the same figure it is possible to observe the exit flow direction and magnitude. It was expected that, as we increase the number of blades, the phase angle also increases. However the 3-bladed rotor is showing a higher phase when compared with the 4-bladed rotor test case. This could be related to the interference effects since in the following solidity test case (pitch of 20 deg) this effect was not present.

A second test case, for pitch amplitude of 20 deg was also performed. Here we intend to analyze if the interference effects are dependent of the blades angle of attack. The power loading vs disk load result for the $\alpha = 20$ deg test cases is shown in Fig. 7. Here is the two bladed rotor that is showing higher values of power loading for the same disk load. For this case we found out that the rotor with 6 blades is the one that produces more trust followed by the rotor with 4 blades. This behavior was not observed in for the pitch amplitude of 40 deg. For the power consumption we can see that, as in the previous case ($\alpha = 40$ deg), the most power consumption is given by the 6 bladed rotor.

4 CONCLUSIONS

In this paper we have performed a parametric study of two different geometrical parameters of cycloidal rotors, namely the blade thickness and the rotor solidity. We can conclude that the rotor efficiency and thrust capability increases with blade thickness. This is mainly due to the fact that flow separation in the top blade position, the one that in principle has the worst behavior because of virtual camber effects, is significantly reduced with the thickness of the airfoil.

For the rotor solidity test case our results show a reduction in efficiency as we increase the number of blades. Also, the interference effects are more evident for higher pitch angles. However the effect of increasing the number of blades, while keeping the rotor solidity constant is not evident. For that an independent study needs to be taken.

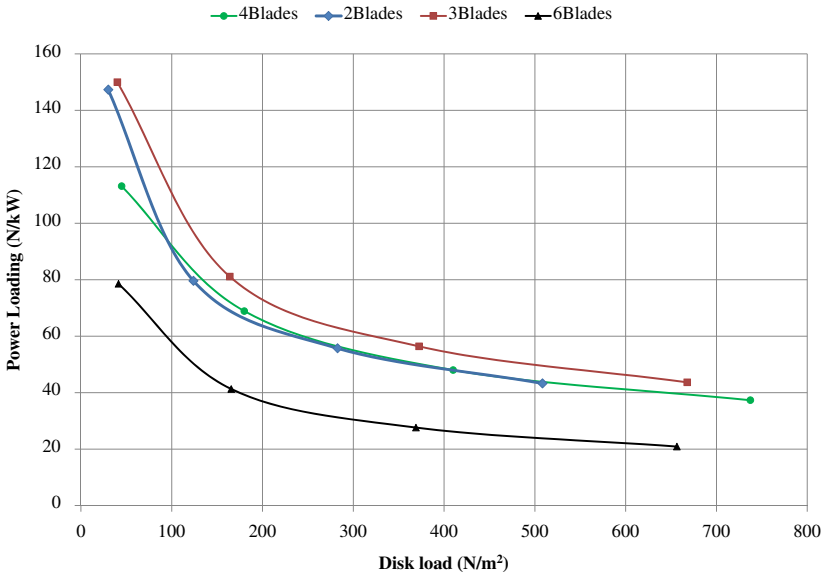

Figure 6: Power Loading vs Disk Load results for the rotor solidity analysis at a pitch amplitude of 40 deg.

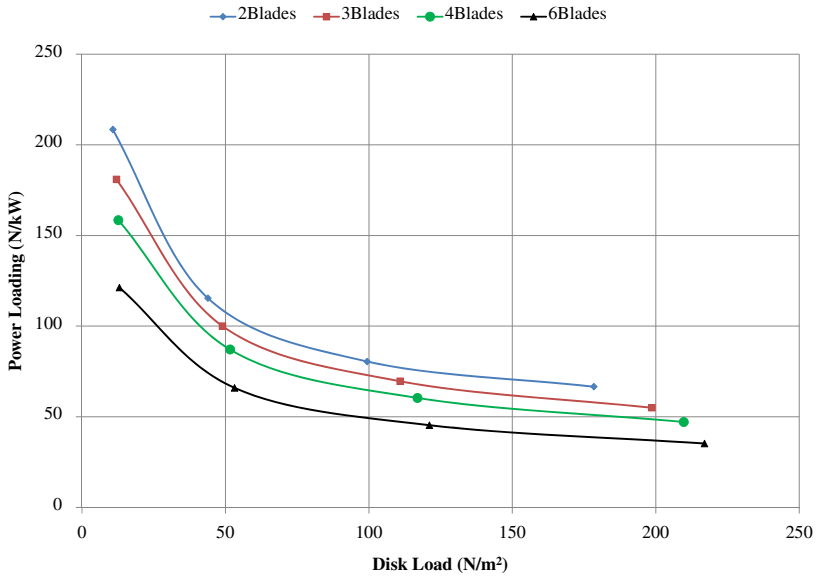

Figure 7: Power Loading vs Disk Load results for the rotor solidity analysis at a pitch amplitude of 20 deg.

5 ACKNOWLEDGMENT

The present work was performed as part of Project CROP, supported by European Union within the 7th Framework Programme under grant number 323047, and also sup-

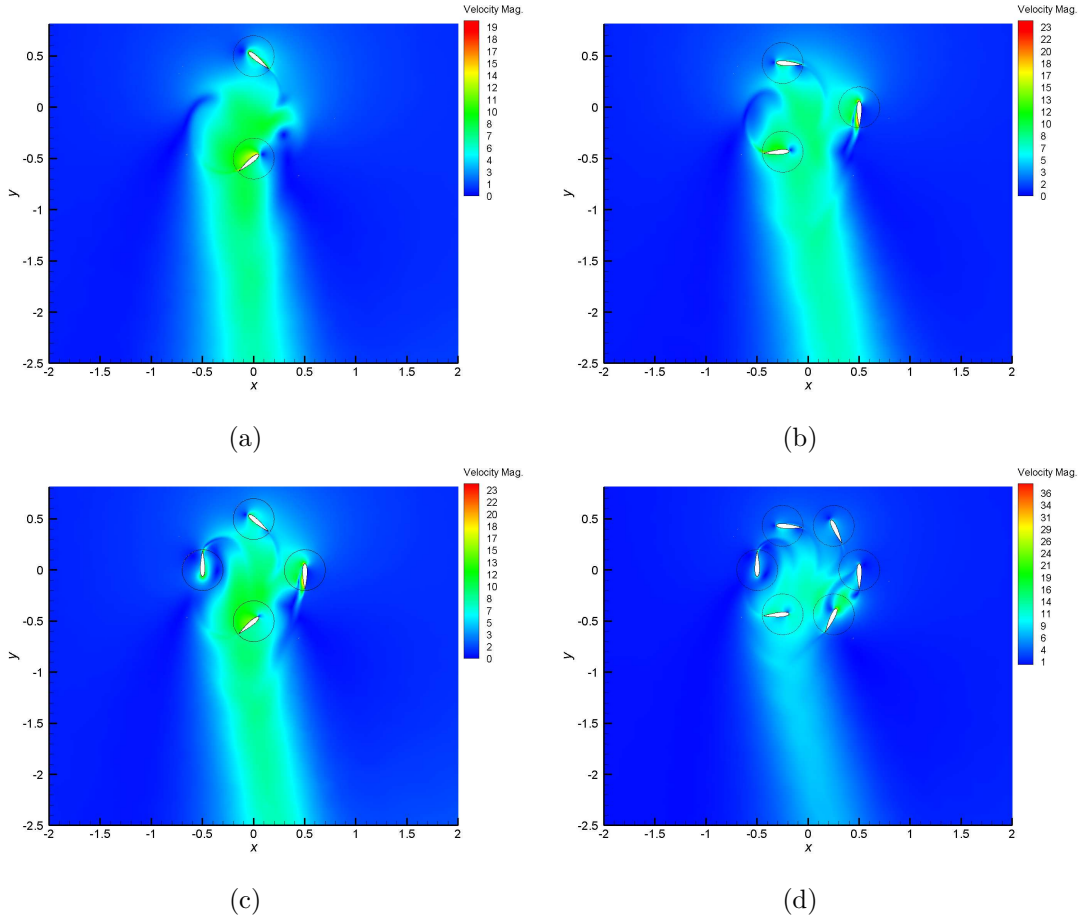

Figure 8:

ported by C-MAST, Centre for Mechanical and Aerospace Science and Technology Research Unit No. 151.

REFERENCES

[1] M. Abdollahzadeh, J.C. Páscoa, and P.J. Oliveira. Two-dimensional numerical modeling of interaction of micro-shock wave generated by nanosecond plasma actuators and transonic flow. *Journal of Computational and Applied Mathematics*, in press(0):–, 2013.

[2] M. Benedict, T. Jarugumilli, and I. Chopra. Effect of Rotor Geometry and Blade Kinematics on Cycloidal Rotor Hover Performance. *Journal of Aircraft*, 50(5):1340–1352, September 2013.

[3] M. Benedict, M. Mattaboni, I. Chopra, and P. Masarati. Aeroelastic Analysis of a Micro-Air-Vehicle-Scale Cycloidal Rotor in Hover. *AIAA Journal*, 49(11):2430–2443,

November 2011.

[4] Moble Benedict. *Fundamental understanding of the Cycloidal-Rotor concept for micro air vehicle applications*. PhD thesis, University of Maryland, 2010.

[5] S. Hwang, Y. Min, H. Lee, and J. Kim. Development of a Four-Rotor Cyclocopter. *Journal of Aircraft*, 45(6):2151–2157, November 2008.

[6] J. Leger, J. Páscoa, and C Xisto. Analytical modeling of a cyclorotor in forward flight. In *SAE 2013 AeroTech Congress & Exhibition*, 2013.

[7] J. Leger, J. Páscoa, and C Xisto. Parametric design of cycloidal rotor thrusters. In *Proc. ASME International Mechanical Engineering Congress and Exposition*, number IMECE2013-65238, 2013.

[8] José C. Páscoa, Carlos M. Xisto, and Emil Gottlich. Performance assessment limits in transonic 3d turbine stage blade rows using a mixing-plane approach. *Journal of Mechanical Science and Technology*, 24(10):2035–2042, 2010.

[9] D. Wills and M. Schwaiger. D-dalus. In *In US EUCOM Science & Technology Conference*, Stuttgart, June 2012.

[10] C. M. Xisto, J. C. Páscoa, M. Abdollahzadeh, J. A. Leger, M. Schwaiger, and D. Wills. Pecyt - plasma enhaced cycloidal thruster. In *50th AIAA/ASME/SAE/ASEE Joint Propulsion Conference*, Cleveland, July 2014.

[11] C. M. Xisto, J. C. Páscoa, P. J. Oliveira, and D. A. Nicolini. A hybrid pressure density-based algorithm for the euler equations at all mach number regimes. *International Journal for Numerical Methods in Fluids*, 70:8:961–976, 2012.

[12] C.M. Xisto, J.C. Páscoa, and P.J. Oliveira. A pressure-based method with ausm-type fluxes for mhd flows at arbitrary mach numbers. *International Journal for Numerical Methods in Fluids*, 72:11:1165–1182, 2013.

[13] Hu Yu, Lim Kah Bin, and Tay Wee. The investigation of cyclogiro design and the Performance. In *25th International Congress of Aeronautical Sciences*, pages 1–5, 2006.